Identification and characterization of a non-conventional CD45 negative perivascular macrophage population within the mouse brain.

Carole Siret
CIML
Max van Lessen
WWU Münster
Hyun-Woo Jeong
Max Planck Institute for Molecular Biomedicine, Department of Tissue Morphogenesis, 48149 Münster, Germany https://orcid.org/0000-0002-6976-6739
Shuaiwei Wang
CIML
Milesa Simic
CIML
Lauriane de Fabritus
CIML
Aurelie Tchoghandjian
Aix-Marseille University
Mathieu Fallet
CIML
Sandrine Sarrazin
CIML
Michael Sieweke
Centre d'Immunologie de Marseille - Luminy, Aix Marseille University, Centre National de la Recherche Scientifique, Institut National de la Santé et de la Recherche Médicale/Max-Delbr https://orcid.org/0000-0002-3228-9537
Ralf Stumm
Jena University Hospital https://orcid.org/0000-0002-9458-5526
Ralf Adams
Max Planck Institute for Molecular Biomedicine https://orcid.org/0000-0003-3031-7677
Stefan Merker
WWU Münster
Friedemann Kiefer

Max Planck Institute for Molecular Biomedicine Department, Vascular and European Institute for Molecular Imaging, University of Munster, Munster

Serge van de Pavert (vandepavert@ciml.univ-mrs.fr)

CIML https://orcid.org/0000-0002-7147-4380

Article

Keywords: brain vasculature, lymphatic vasculature, inflammation, drainage, whole mount imaging, stroke, photothrombosis, perivascular macrophages

Posted Date: May 19th, 2021

DOI: https://doi.org/10.21203/rs.3.rs-479980/v1

Identification and characterization of a non-conventional CD45 negative perivascular macrophage population within the mouse brain.

C. Siret[1], M. van Lessen[2], H. W. Jeong[3], S. Wang[1], M. Simic[1], L. de Fabritus[1], A. Tchoghandjian[4], M. Fallet[1], S Sarrazin[1], M.H. Sieweke[1,5], R. Stumm[6], R. H. Adams[3], S. Schulte-Merker[2], F. Kiefer[3,8], S.A. van de Pavert[1,] *****

[1] Aix-Marseille Univ, CNRS, INSERM, Centre d'Immunologie de Marseille-Luminy (CIML), Marseille, France

[2] Institute for Cardiovascular Organogenesis and Regeneration, Faculty of Medicine, WWU Münster, Mendelstrasse 7, 48149 Münster, Germany

[3] Max Planck Institute for Molecular Biomedicine, Münster, Germany.

[4] Aix-Marseille Univ, CNRS, INP, Inst Neurophysiopathol, Marseille, France.

[5] Center for Regenerative Therapies Dresden (CRTD), Technische Universität Dresden, 01307 Dresden, Germany

[6] Institute of Pharmacology and Toxicology, Jena University Hospital, Jena, Germany

[8] European Institute for Molecular Imaging - EIMI, Westfälische Wilhelms-Universität Münster, Münster, Germany.

*** Correspondence:**

Serge van de Pavert; vandepavert@ciml.univ-mrs.fr

Keywords: brain vasculature, lymphatic vasculature, inflammation, drainage, whole mount imaging, stroke, photothrombosis, perivascular macrophages

ABSTRACT

Perivascular macrophages (pvM) are closely associated with cerebral vasculature and play an essential role in drainage of the brain and regulation of the immune response. Here, using reporter mouse models and immunofluorescence on sections and whole brain, flow cytometry and single cell sequencing, we identify a Lyve1^{+} brain perivascular population lacking classical macrophage markers such as CD45 and Cx3cr1. We named the new non-conventional CD45 negative perivascular macrophages pvM2. These cells have a similar location, morphology and phagocytic function as conventional pvM. The pvM2 are not derived from hematopoietic stem cells, as they are negative in the *Vav*^{tdT} lineage tracing model. They increase in number after photothrombotic induced stroke established by flow cytometry and 3D immunofluorescence analysis. Since CD45 negative cells were typically excluded from macrophage studies, the presence of pvM2 has been previously missed and their role is of importance to assess in the brain disease models.

INTRODUCTION

The central nervous system (CNS) has long been considered immune privileged, devoid of immune cells other than microglia and without classical lymphatic vessels. The re-discovery of the dural lymphatic network highlights a route for the drainage of the brain to the periphery [1–6]. How drainage from the CNS parenchyma occurs towards lymphatics and draining lymph nodes is unknown, but there are indications this happens via the foramen at the base of the skull [3].

Besides microglia, several myeloid populations have now been characterized and shown to be essential for brain homeostasis and in brain diseases [7]. These myeloid populations include the so-called non-parenchymal or border macrophages which can be classified in the perivascular, subdural meningeal and choroid plexus macrophages. These macrophages are established during development by embryonic precursors derived from yolk sac precursors and are not replaced by blood monocytes during adulthood, except for the choroid plexus macrophages [8]. Specifically, perivascular macrophages (pvM) are located in the perivascular space of the blood vessel, delimited by the vascular basement membrane of blood vessels and glial basement membranes [9]. The pvM have been shown to be involved in many processes within the CNS. Early studies demonstrated that pvM are capable of scavenging molecules injected into the cerebral ventricles. They contribute to the blood brain barrier function and mediate the up-take of macromolecules [10–12], participate in immune regulation [13]. They are involved in a wide variety of brain related disorders such as cerebrovascular and neurocognitive functions in hypertension [14], brain infections, immune activation, Alzheimer's disease [15,16] and multiple sclerosis

[17,18], suggesting that they are a key component of the brain-resident immune system and involved in clearing or draining of the CNS.

Lyve1 is notably expressed on lymphatic endothelial cells (LEC) and macrophages, but not on microglia. Specifically, distinct macrophage populations lining the blood vessels within the periphery have been characterized as Lyve1^{hi} and Lyve1^{lo} [19]. In the mouse brain, myeloid cells are a heterogeneous group of cells localized in specific niches and include parenchymal microglia and non-parenchymal pvM [7,20]. Previously, brain pvM were described to be CD45^{+} and were shown to express canonical macrophage markers such as fractalkine receptor (Cx3cr1), colony-stimulating factor1 receptor (Csf-1R), CD206 and Iba-1, but also the prototypic macrophage markers CD11b and F4/80 [7,8].

Recent studies highlighting Lyve1^{hi} and Lyve1^{lo} pvM [19], peripheral nervous system and specific border-associated macrophages [21,22] have shown that the macrophage population within the nervous system is heterogenous. However, all these studies have excluded CD45^{-} cells. In the current study, using different reporter- and fate-mapping mouse models and employing both (whole-mount) immunofluorescence as well as flow-cytometry and single cell sequencing, we observed a previously uncharacterized CD45^{-}CX3CR1^{-}PU.1^{-}Lyve1^{+}F4/80^{+} cell population within the mouse brain. We established that these cells were not lymphatic endothelial cells, but non-conventional pvM lining blood vessels, having a similar morphology as conventional pvM. Functionally, they were able to phagocytose macromolecules injected within the ventricle. During photothrombotic-induced stroke, CD45^{-} pvM increased similar as conventional pvM. Hence, our data characterize a previously overlooked CD45^{-} pvM cell population, which we name non-conventional CD45^{-} perivascular macrophages (pvM2).

RESULTS

Identification of a Lyve1$^+$CX3CR1$^-$ cell population in the brain parenchyma

Using whole-mount immunofluorescence of the superior and inferior cortex and cerebellum, we identified Lyve1$^+$ cells that did not form lymphatic luminized vessels (Fig. 1A-D, whole brain in Video 1 and maximum intensity projection in Supplementary Fig. 1A). Their cellular morphology depended on their location. Within the superior cortex (Fig. 1A) they were small and spread, similar as in the pia mater. Within the inferior cortex, these cells were elongated and more stretched, as they were also within the hippocampus (Fig. 1B-C)**.** In the olfactory bulb, near the cribriform plate, where cerebrospinal fluid (CSF) lymphatic drainage occurs from the sub-arachnoid space into nasal lymphatics, Lyve1$^+$ cells were also found to be long and stretched (Fig. 1D).

In *Cx3cr1*$^{GFP/+}$ and *Spi1*$^{GFP/+}$ (gene encoding PU.1) mouse brain sections, we identified conventional Lyve1$^+$CX3CR1$^+$F4/80$^+$Iba1$^+$ pvM (white arrows in Fig. 1). In addition, we observed a Lyve1$^+$CX3CR1$^-$ population expressing F4/80 and Iba1 (Fig. 1E, F) but lacking classical hematopoietic and other macrophage markers such as CD45, Csf1-R and PU.1 (red arrows in Fig. 1E-I), which has not been described before. We confirmed the lack of CX3CR1 and PU.1 on sections using an anti-GFP (Supplementary Fig. 1B,C). Furthermore, these atypical Lyve1$^+$CX3CR1$^-$ cells lacked CD163, CD206, MHCII and CD11b expression (Supplementary Fig. 1D-G). The pvM markers expressed are summarized in Table 2.

Lyve1$^+$CX3CR1$^-$ cells are non-conventional CD45$^-$ perivascular macrophages (pvM2)

In the light of the recent re-discovery of lymphatic vessels in the meningeal compartment [1,6,32], we investigated whether the Lyve1$^+$CX3CR1$^-$CD45$^-$ population in the parenchyma of adult mice was of lymphatic origin. We observed Lyve1$^+$ cells in very close association with blood vessels (Fig. 2A-D, Video 2) and located outside of a structure called “pia mater cul de sac” (Fig. 2B-D). The pia mater formed invaginations into the brain parenchyma, visualized by Podoplanin [9], surrounding arterioles within the cortex. We observed that the Podoplanin$^+$ pia was located between the vascular endothelium and the Lyve1$^+$ cells (Fig. 2B-D, Supplementary Fig. 2A). We also observed that the Lyve1$^+$ cells were positioned within the Laminin γ1$^+$ endothelial cell basement membrane within the perivascular space (Fig. 2E-F). This compartment is defined by the vascular basement membrane on the abluminal side of the vessel wall and by the glia limitans basement membrane on the parenchymal side [33]. We observed that Lyve1$^+$ cells did not express CD31 (Fig. 2A-H), Podoplanin (Fig. 2B-D), VEGFR3 (Fig. 2G-H) or master-regulator for lymphatic endothelial identity Prox1 (Fig. 2I-L), ruling out a lymphatic identity. We verified non-lymphatic phenotype using *Prox1*^{mOrange2} (Supplementary Fig. 2B-C) and

Prox1^{CreErt2};*Rosa26*^{tdT} (Supplementary Fig. 2D) reporter mouse models [24,34]. We analyzed the *Prox1*^{CreErt2};*Rosa26*^{tdT} brain 2 weeks after Tamoxifen injection and did not observe *Prox1*$^{+}$ lymphatic endothelial cells, ruling out any LEC identity within the brain parenchyma (Supplementary Fig. 2B). While the dura mater contains lymphatic vessels, no conventional lymphatics have been described within the parenchyma nor the leptomeninges. Similarly, while we did not observe luminized lymphatic vessels within the pia mater, we did find single Lyve1^{+}Prox1^{+} lymphatic endothelial cells in the pia mater (Supplementary Fig. 2B-C) as was also recently described in mammals [35].

To further rule out astrocyte, glial or fibroblast identity, we analyzed immunofluorescence staining for Aquaporin-4 (AQP4) and GFAP (Supplementary Fig. 2D), ER-TR7 (Supplementary Fig. 2E), PDGFRβ (Supplementary Fig. 2F) and observed these cells to be negative for all. Furthermore, we excluded neural crest cell origin using the *Wnt1*^{Cre}; *Rosa26*^{tdT} reporter mouse model (Supplementary Fig. 2G).

We confirmed the presence of the Lyve1^{+}CD45^{-} populations at different stages during life by flow cytometry. Using *Cx3cr1*^{GFP} brain parenchyma cell suspension devoid of meninges, conventional pvM were identified as Lyve1^{+}CD45$^{int/high}$ while microglia were excluded as they are Lyve1^{-}(gating strategy in Supplementary Fig. 3A). These Lyve1^{+}CD45^{-} cells also lacked CX3CR1, confirming IF section stainings (Fig. 1). After 2 days after birth (P2) we observed a Lyve1^{+}CD45^{-}CX3CR1^{-}F4/80^{+} population which peaked at P14 and P21(Fig. 3A-D). Subsequently, we observed lowered numbers in adult and 1-year old brain parenchyma (Fig. 3E-F, absolute Lyve1^{+}CD45^{-}CX3CR1^{-}F4/80^{+} cell numbers in Fig. 3G). Also in the *Spi1*^{GFP} (encoding PU.1) brain parenchyma we observed a CD45^{-} PU.1^{-}F4/80^{+} population, next to the conventional CD45$^{int/high}$ populations (Supplementary Fig. 3C), albeit less Lyve1^{+}CD45^{-}PU.1^{-} F4/80^{+} cells were present compared to the Lyve1^{+}CD45^{-}CX3CR1^{-} population observed in the *Cx3cr1*^{GFP} brain parenchyma.

We confirmed absence of *Ptprc* (encoding CD45) expression within the Lyve1^{+}CD45^{-} cells by sorting this population and determination of *Ptprc* mRNA levels by qPCR and observed no *Ptprc* expression within the Lyve1^{+}CD45^{-} population (Fig. 4A, sorting strategy in Supplementary Fig. 4A). To further characterize the transcriptome of the pvM population, we analyzed the single cell RNA sequencing dataset of the non-neuronal cell population in mouse brain cortex (GSE133283), thus including the CD45^{-} cells (Fig. 4B, C). We identified macrophages expressing the characteristic macrophage markers *Mrc1*, *Cd68* and *Fcgr3* (Fig.S4B). This macrophage cluster was segregated into at least two subtypes; *Lyve1*$^{+}$ and *H2-Aa*$^{+}$ (one of the genes encoding MHCII) (Fig.4C). We observed cells with

lower or undetectable *Ptprc* or *Cx3cr1* expression and fewer cells with lower *Spi1* expression (Fig.4C). However, these cells were not segregated from other cells by unsupervised clustering analysis, confirming their identity as macrophages.

Since we ruled out a lymphatic identity, established that the cells expressed macrophage markers and clustered together with the conventional pvM in the single cell sequencing, we name these cells non-conventional CD45^{-} perivascular macrophages (pvM2).

PU.1 is considered to be a master regulator for macrophage differentiation. Therefore, we analyzed the *Spi1*$^{GFP/GFP}$ mouse model, in which GFP is knocked into the *Spi1* locus (encoding PU.1) rendering this gene inactive. Homozygous mice deficient for *Spi1* lack all macrophages and die around birth [8,27]. In E18.5 *Spi1*$^{GFP/+}$ embryos, we identified Lyve1^{+}PU.1^{+}CD45^{+} and Lyve1^{+}PU.1^{-}CD45^{-} pvM (pvM2) (Fig. 5A) while in E18.5 *Spi1*$^{GFP/GFP}$ (knock-out) embryos we observed a total absence of Lyve1^{+} cells in the brain parenchyma (Fig. 5B, positive staining of Lyve1^{+} cells in the skull in Supplementary Fig. 5). This demonstrates that Lyve1^{+}CD45^{-} depend on PU.1 during their development, but lose expression during life (Supplementary Fig. 3C).

We tested a possible hematopoietic stem cell (HSC) – bone-marrow derived hematopoietic origin of this population using the *Vav*^{Cre}*; Rosa26*^{tdT} (hereafter named *Vav*^{tdT}) reporter mouse model. *Vav* expression starts around embryonic day 8.5 (E8.5) in the hemogenic endothelium of the dorsal aorta in aorta-gonad-mesonephros (AGM) region, which gives rise to the HSC and monocytes [36]. By immunofluorescence staining of *Vav*^{tdT} brain sections, we identified a Lyve1^{+}CD45^{+}Vav-lineage^{+} and a Lyve1^{+}CD45^{-}Vav-lineage^{-} population (Fig. 5C). Therefore, we concluded that the Lyve1^{+}CD45^{-} cells were not derived from HSC or bone-marrow derived monocytes.

Phagocytosis by pvM2

Besides their role as source for chemokines and growth factors to regulate an immune response, pvM have a phagocytic function, which could be part of a broader role of these cells for tissue homeostasis [19,37]. In order to address a role of the pvM2 in fluid drainage or macromolecule clearance, we injected 10kD Dextran-AlexaFluor647 and Acetylated LDL-AlexaFluor594 in the lateral ventricle of *Cx3cr1*^{GFP} mouse brains. To exclude recirculation through the blood stream, we analyzed the brain 10 minutes after injection [3]. We observed that both Lyve1^{+}CX3CR1^{-} and Lyve1^{+}CX3CR1^{+} cells phagocytized the injected dyes near the ventricle, in the superior- (Fig. 6A-C) and in the inferior cortex (Fig. 6D-F). We concluded that Lyve1^{+}CX3CR1^{-} cells were able to efficiently take up lipoproteins and glycoproteins in the range of at least 3 to 10kDa similar as conventional pvM. The close proximity of the pia mater extending towards the third ventricle (3V) could explain direct drainage from the

injection-site within the lateral and connected 3V towards the pia mater (Fig. 6G). Very few Lyve1 and Prox1mOrange2 positive nuclei were observed within the pia mater (Fig. 6G).

Involvement in central nervous system diseases

It was shown that in stroke pvM can influence the blood-brain-barrier function [38,39]. In patients with intracerebral hemorrhage and focal cerebral ischemia, a $CD163^+$ cell accumulation around brain blood vessels was observed, which also contained myelin [40]. Moreover, it was not clear whether these cells are blood-derived monocytes or pvM since they were not characterized in detail (Holfelder K. *et al*., 2011).

To assess the role of the pvM2 in cerebrovascular pathologies, we investigated a photothrombotic model of ischemic stroke. PT was induced on 8 weeks old male mice. In this model, we observed an increase in Lyve1 staining density in whole-mount stained brains (Fig. 7A, method for quantification of staining density in whole mount brain shown in Supplementary Fig. 6A). At day 14 post stroke induction (P14), we noticed a significant increase of Lyve1 staining density (4.2x, $p<0.05$) within the hippocampus, although no significant difference was observed in the superior cortex. At P30, Lyve1 staining density had normalized to control values again (Fig. 7B). We noted an increase in the total $Lyve1^+$ population, including $CD45^{int}$ and $CD45^-$ population by flow cytometry (Fig. 7C). The relative numbers of the $CD45^{int}$ and $CD45^-$ populations remained similar compared to the control (not shown), but the absolute number of $CD45^-Lyve1^+F4/80^+$ pvM2 increased in PT (Fig. 7D, E and Supplementary Fig. 6B).

DISCUSSION

We have carefully examined whether lymphatic endothelial cells exist within the central nervous system. However, thorough analysis of different reporter mouse models did not reveal these cells within the parenchyma and few individual lymphatic endothelial cells were observed only within the pial meninges as described before [35]. Using flow-cytometry, single cell, immunofluorescence and lineage-tracing models, we characterized a novel perivascular cell population and named it non-conventional CD45^{-} perivascular macrophages (pvM2). This population did not express several classical macrophage markers but still clustered together with other macrophages in single cell sequencing analysis. It closely resembled conventional pvM, in location and function. Similar as pvM, pvM2 located outside the cul-de-sac of the pia-mater and within the Virchow-Robin space, which is likely to be associated with their functioning in drainage [8,39,41]. Classical brain pvM are derived from the yolk-sac hemogenic endothelium and depend on Csf1R during their maturation [8]. Based on the absence of labeling in the *Vav1^{tdT}* model, we conclude that pvM2 are not bone-marrow derived monocytes. As was shown for pvM in the periphery [19], pvM2 are also most likely derived from the yolk-sac. Using the *Spi1* reporter (encoding the PU.1 protein) and knock-out model, we demonstrate that, similar to myeloid cells, they require PU.1 for differentiation but not for maintenance. They could still have the *Spi1* mRNA transcripts, but not he protein or GFP reporter, as we observed more cells positive for *Spi1* than for *Cx3cr1* or *Ptprc* in the single cell sequencing analysis. It was previously noted that some macrophages originated from CX3CR1^{+} precursors but ceased to express *Cx3cr1*, such as alveolar macrophages, Langerhans and Kupffer cells. These CX3CR1^{-} cell coincided with CX3CR1^{+} cells [42], as we also observed in the brain parenchyma. Why pvM2 lacked Csf1R and thus likely do not require Csf1 for maintenance is yet unclear. Further experiments using other lineage tracing models are required to reveal their exact origin in relation to the differentiation of conventional pvM. It was observed before that non-hematopoietic ectodermal cells gave rise to phagocytosing cells, resembling Langerhans cells, in the skin of zebrafish [43]. However, it was not shown that these cells depend on PU.1 and moreover were located within the skin of the zebrafish. Whether these cells resemble the murine pvM2 is yet unclear.

In adult tissues at steady-state, pvM have important functions related to their perivascular location, such as the regulation of vascular permeability, phagocytosis of blood-transmissible pathogens, antigen presentation or immune regulation [37]. Here, we observed similar phagocytosis of the pvM2 when compared to conventional pvM. Previously, two perivascular monocyte populations were described, being Lyve1^{hi} or Lyve^{lo}. MHCII was expressed high on the Lyve1^{lo} population while the Lyve1^{hi} population was MHCII low [19]. However, in past studies both Lyve1^{hi} or Lyve^{lo} populations were gated

only from $CD45^+$ cells. CD45 negative non-conventional pvM, if present, were disregarded. Since the pvM2 did not express CD45, MHCII nor CX3CR1, but were $Lyve1^+$, it is not clear how these cells relate to the previously described perivascular monocytes.

Using whole-mount imaging enabled us to establish the pvM contribution specifically within and adjacent to the affected region in ischemic stroke. We established an increase in the total pvM number after stroke, with a concomitant significant increase of the pvM2 population. As the number of the pvM2 increases during stroke, these cells may be involved in the generation of an activated immune status. All previous studies on pvM within the brain analyzed $CD45^+$ cells. This study now for the first time presents evidence of a $CD45^-CX3CR1^-$ population, named pvM2, which is present within the brain and should be considered in the future to better understand the active role of diverse macrophage populations in brain homeostasis and disease.

In conclusion, here we demonstrate the existence and function of non-conventional $CD45^-$ pvM2, lacking classical macrophage makers such as CD45, CX3CR1, PU.1, CD206, CD163 and CD11b. These cells are consistently observed within the brain and are likely involved in drainage also due to their blood vessel proximity and involved in an activated immune state such as during ischemic stroke. Although these novel pvM2 increase in number during stroke, their specific role during disease remains unclear. Presently, there are no unique markers available to target these cells specifically, but a newly developed marker should allow a targeted approach to study their specific role in brain physiology in the future.

METHODS

Mice

C57BL/6J and *Vav1-Cre* [23] mice were obtained from Charles River [France]. *Prox-CreERT2*$^{+/-}$ [24] and *Wnt1-Cre* [25] mice were kindly provided by Dr. Bajénoff (CIML, Marseille, France). *Cx3cr1*^{GFP} mice [26] were kindly provided by Dr. Lelouard (CIML, Marseille, France). *Spi1*^{GFP} (PU.1) [27], *Csf1R-Cre* [28] and *Prox1*^{mOrange2} [29] were maintained at the CIML (Marseille, France).

Vav1-Cre, *Prox-CreERT2*$^{+/-}$, *Wnt1-Cre* and *Cx3cr1-Cre* lines were crossed to homozygosity for the tdTomato reporter using Rosa26^{tdT} mice [30]. 5 mg of Tamoxifen was injected IP to a *Prox-CreERT2*$^{+/-}$.Rosa26^{tdT} adult 2 weeks before the isolation of the brain. All experiments were reviewed and approved by the local ethics committee of Aix-Marseille University and the Ministère de l'Enseignement Supérieur, de la Recherche et de l'Innovation.

Antibodies Table 1

Cell preparation and flow cytometry

Cx3cr1^{GFP} mouse brains from male mice were collected after perfusion with ice cold PBS-Heparin (after removal of the dura). Brains were cut sagitally in 6-8 pieces, then digested with the Adult Brain Dissociation Kit (Miltenyi, 130-107-677) at 37°C for 30min on the gentleMACS dissociator (Miltenyi). Brain cell suspensions were filtered over 70µm strainers and filters were washed with 10mL HBSS 2%FBS. After centrifugation (5min, 400g, 4°C), debris were removed using a 40% Percoll (Sigma-Aldrich, GE17-0891-02) solution in PBS. Cells were centrifuged (30min, 500g, 4°C) and supernatant was discarded. Red blood cell lysis was performed for 10 min at 4°C using the Miltenyi RBC lysis buffer from the kit. Lysis was stopped with 9mL HBSS 2%FBS and cells were centrifuged (5min, 400g, 4°C). Cells were then blocked (15% normal mouse serum (Jackson Immunoresearch 015-000-120) in FACS buffer (HBSS 2% FBS) for 15 min and subsequently stained for CD45-BUV395 (BD biosciences 564279), Lyve1-eFluor660 (eBioscience 50-0443-82) and F4/80-BV421 (Biolegend 123131) diluted in FACS buffer for 30min on ice. The staining of dead cells with Fixable NIR was performed for another 30 min after the antibody staining in protein free HBSS right after washing the cells. Cells were subsequently washed and resuspended in FACS buffer. Samples were acquired on the LSRFortessa X-20 cytometer (BD Biosciences). Data analyses were done using FlowJo software (version 10, FlowJo, LLC).

Cell sorting

Cells were prepared and stained with CD45, and Lyve1 antibodies and Fixable NIR as describe above. Live Lyve1^{+} CD45^{-}, live Lyve1^{+} CD45^{int} and live Lyve1^{+} CD45^{high} cells were sort-purified separately using the BD FACS ARIA III SORP sorter.

RNA isolation and gene expression analysis

After spinning down (7min, 300g, 4°C), cells were resuspended in 1mL TRIzol reagent (Sigma T9424). The suspension was transferred to a phase lock gel heavy tube to facilitate the extraction and 200µL of chloroform was added. The samples were shaken vigorously and incubated for 3 min at room temperature (RT) prior to centrifugation (10min, 12 000g, 4°C). The clear aqueous phase was transferred to a new tube and 2µL of GlycoBlue Coprecipitant (Invitrogen AM9515) was added to help with the isolation prior to adding 500µL of isopropanol. The samples were incubated for 10min at RT and subsequently centrifuged (30min, 12 000g, 4°C). The supernatant was discarded and RNA was washed with 800µL EtOH 70%. The samples were centrifuged (5min, 12 000g, 4°C) and supernatants were discarded. The RNA was air-dried for 15min prior to resuspension in 11.5µL RNase free water. The tubes were subsequently heated at 65°C for 10min and then put on ice. RNA quantity and quality were assessed by nanodrop. For each sample, 200ng of RNA was reverse transcribed using the RevertAid Reverse Transcription kit (Thermo Scientific K1691) and adding Oligo $(dT)_{12-18}$ primer (Invitrogen, 12418012). The level of expression of CD45 (Forward CCCCGGGATGAGACAGTTG; Reverse AAAGCCCGAGTGCCTTCCT) gene was assessed by qPCR using Sybr Green (Takara, TAKRR420W) and Hprt was used as reference gene (Forward GGCCAGACTTTGTTGGATTT; Reverse CAGATTCAACTTGCGCTCAT). Data were analyzed using the delta-delta Ct method and compared to the CD45^{-} fraction.

Single cell RNA sequencing data of non-neuronal cell populations in mouse brain cortex was adapted from GSE133283 (unpublished). Mrc1-expressing perivascular macrophage population was isolated and reanalysed using Seurat (version 3.2.1) R package. Variable genes were found with parameters of selection.method = vst and nfeatures = 2,000, trimmed for the genes related to cell cycle (GO:0007049) and then used for principal component analysis (RunPCA , npcs=30). Statistically significant principal components were determined by JackStraw method and the first 5 principle components were used for non-linear dimensional reduction (RunTSNE) and clustering analysis (FindNeighbors) with resolution=0.1. FeaturePlot function was used to visualize the specific gene expression on TSNE plot. Blue represents the relative expression level of each gene.

Whole-mount staining and lightsheet imaging

Both male and female mice were perfused with PBS-Heparin 5U/ml (Sigma) and subsequently overnight (ON) immersion fixed in paraformaldehyde 4% (PFA-Electron Microscopy Science, ref

15714) in PBS. The iDISCO protocol was used for immuno-staining [31], prior to which brains were dehydrated in increasing methanol (MetOH) concentrations diluted in PBS (20, 40, 60, 80 and twice 100%) for 30 minutes for each concentration at RT. Subsequently specimens were incubated ON in a dichloromethane (DCM, Sigma 270997)-MetOH mixture (2 vol DCM:1 vol MetOH) at RT. After two 10 minutes incubations in absolute MetOH, brains were bleached in 5% H_2O_2 in MetOH ON at 4°C and subsequently rehydrated by a decreasing MetOH series (80, 60, 40, 20% in water), followed by PBS and two washes in PBS-Triton X100 (Tx) 0.2% for 1 hour each. Bleached brains were permeabilized for 2.5 days at 37°C (0.4%Tx, 20%DMSO, 2.3% Glycine in PBS) and subsequently blocked with [PTwH (PBS, Tween20, Heparin), 10% DMSO, 6% serum] for 4.5 days at 37°C. Whole-mount stainings were performed by incubation with primary antibodies for 5 days at 37°C and subsequently with Alexa-dye coupled secondary antibodies diluted in PTwH containing 3% serum for 5 days at 37°C. Following each staining step, samples were extensively washed in PTwH (10min, 15mn, 30min,1h, 2h, and ON at RT). Finally, the samples were again dehydrated by increasing MetOH concentrations diluted in water (20, 40, 60, 80, 2x 100% and ON in absolute MetOH), for 1 hour each step at RT and cleared in a MetOH/BABB mix (1:1) [BABB (benzyl alcohol and benzyl benzoate = 1:2) (Sigma 305197 and Fisher Scientific 10654752)] for 8 hours at RT and finally placed in BABB ON at RT to complete clearing. All incubations were done under mild agitation. After clearing, brains were imaged using a LaVision Ultramicroscope II (LaVision BioTec, Bielefeld, Germany). Stacks were captured with a step size of 5µm at 2.5X magnification using an optic zoom with a NA=0.144. 3D reconstruction, cell counting and analysis of the sample image stacks were performed using IMARIS software (Version 9.1.0, Bitplane). For Lyve1 quantification, an area of interest was selected (Superior cortex, Hippocampus) using the program's surface function and then a new channel corresponding to the fluorescence to quantify was created in this region. Using this workflow, a quantification of volume (in μm^3) of Lyve1 stained material is possible, which was further adapted for volumetric quantifications (Supplementary Fig. 6).

Vibratome section immunofluorescence staining and confocal imaging

Animals were perfused with PBS/heparin, brains dissected and fixed ON in 4% PFA in PBS at 4°C and subsequently embedded in 1% low melting agarose for generation of 100µm vibratome slices (Leica, VT1000S). Sections were blocked in EBT buffer (EBSS, 0.05% Tx, 1% BSA) containing 10% serum for 2h at RT under agitation. Immunostainings were performed by incubation in primary antibodies for 48h at 4°C in EBT, 3% sera and subsequently with Alexa-fluorochrome coupled secondary antibodies diluted in EBT, 3% sera for 24h at 4°C. Following each staining step, samples were washed several times in PBS-Tx (0.05% Tx in PBS) and in PBS. Sections were finally cleared in

Histodenz (Sigma D2158) medium for 48h at RT and subsequently mounted in Histodenz medium. Confocal images were acquired at RT on a confocal microscope (LSM880, Zeiss, Germany), with a 20x/0.4 Plan-Apochromat objective and using laser lines at 405, 488, 561, and 633nm for the excitation of AlexaFluor405/GFP/AlexaFluor555/AlexaFluor647 respectively. Fluorescence was recorded in individual channels acquired in a sequential mode using a highly sensitive 32-channel GaAsP detector. Channels were respectively detected using these detection bands: A405 (410-470nm), A488 (490-540nm), A555 (565-640nm), A647 (640-690nm). The pinhole was set to 1 airy unit. Z stack were acquired with an optical thickness defined for each image in figure legends, satisfying the Nyquist resolution criterion. Image processing (contrast enhancement, scale bars, etc.) was done with ImageJ (National Institutes of Health) without actions modifying image integrity.

Infusion of tracers into lateral ventricle

Both female and male mice were anesthetized (150mg/kg Ketamine and 10mg/kg Xylazine) and fixed in a stereotaxic frame. The skull was thinned with a dental drill at a location of 0.95 mm lateral and 0.22 mm caudal from the bregma. A 30G needle with a silica fiber tip (Phymed) was inserted into the right lateral ventricle 2.35 mm ventral to the skull surface as previously described [3]. Injection of 2.5 µL acetylated LDL-Alexa594 (ThermoFisher) or Dextran-Alexa647 10kDa (ThermoFisher) tracer was done at a speed of 0.5 µL/min using a high precision syringe pump. The needle was left in place for 5 minutes and slowly retracted confirming lack of detectable backflow. To avoid recirculation through the blood stream into the brain, mice were sacrificed 10 min after injection [3]. The mice were perfused with PBS and 4%PFA/PBS, brains isolated and fixed ON in 4% PFA/PBS at 4°C, subsequently washed and then stored at 4°C in PBS until further analysis.

Photothrombotic (PT) induced stroke

Stroke using the PT model was induced in male C57BL/6J and *Cx3cr1*^{GFP} mice. Mice were anesthetized by intraperitoneal Ketamine/Xylazine injection as before and the eyes of the mice were covered with Ocry-gel to protect them from light and dehydration. The skin on the skull was incised from the eyes to the neck and retracted to the edges of the skull. After retro-orbital injection of 100 µL Rose Bengal (Sigma, 330000) a Leica, KL 1600LED cold light source was placed in contact with the skull and the illuminated region was precisely adjusted (using a stereotaxic instrument) to 2.5 mm caudal of the Bregma and 2.0 mm to the Lambda. After illuminating a 1 mm diameter area at power 3 for 15 minutes, the skin was put back into place, stitched and the animals returned to their home cages. Food was provided in a plate and Buprenorphine (0.4 mg/ml) was added to the drinking water. Mice were sacrificed between 14- and 30-days post-induction and brains were analyzed by immunofluorescence and flow cytometry.

Statistical analysis

Graphs, average values and standard deviation (SD) shown in all figures were calculated using Prism (version 8.3.0 GraphPad software) software. Unpaired T-Test and One-way Anova test were used to determine significance. The number of individual experiments can be found in the legends of all the figures. Photoshop software (CC2015, Adobe) was used to generate figures.

REFERENCES

1. Aspelund, A. *et al.* A dural lymphatic vascular system that drains brain interstitial fluid and macromolecules. *J. Exp. Med.* **212**, jem.20142290- (2015).
2. Ahn, J. H. *et al.* Meningeal lymphatic vessels at the skull base drain cerebrospinal fluid. *Nature* (2019). doi:10.1038/s41586-019-1419-5
3. Ma, Q., Ineichen, B. V., Detmar, M. & Proulx, S. T. Outflow of cerebrospinal fluid is predominantly through lymphatic vessels and is reduced in aged mice. *Nat. Commun.* **8**, 1434 (2017).
4. van Lessen, M. *et al.* Intracellular uptake of macromolecules by brain lymphatic endothelial cells during zebrafish embryonic development. *Elife* **6**, (2017).
5. Absinta, M. *et al.* Human and nonhuman primate meninges harbor lymphatic vessels that can be visualized noninvasively by MRI. *Elife* **6**, e29738 (2017).
6. Louveau, A. *et al.* Structural and functional features of central nervous system lymphatic vessels. *Nature* (2015). doi:10.1038/nature14432
7. Prinz, M., Erny, D. & Hagemeyer, N. Ontogeny and homeostasis of CNS myeloid cells. *Nat. Immunol.* **18**, 385–392 (2017).
8. Goldmann, T. *et al.* Origin, fate and dynamics of macrophages at central nervous system interfaces. *Nat. Immunol.* **17**, 797–805 (2016).
9. Zhang, E. T., Inman, C. B. & Weller, R. O. Interrelationships of the pia mater and the perivascular (Virchow-Robin) spaces in the human cerebrum. *J. Anat.* **170**, 111–123 (1990).
10. Mato, M., Ookawara, S. & Kurihara, K. Uptake of exogenous substances and marked infoldings of the fluorescent granular pericyte in cerebral fine vessels. *Am. J. Anat.* **157**, 329–332 (1980).
11. Mato, M. *et al.* Involvement of specific macrophage-lineage cells surrounding arterioles in barrier and scavenger function in brain cortex. *Proc. Natl. Acad. Sci.* **93**, 3269 LP – 3274 (1996).
12. Bechmann, I. *et al.* Immune surveillance of mouse brain perivascular spaces by blood-borne

macrophages. *Eur. J. Neurosci.* **14**, 1651–1658 (2001).
13. Fabriek, B. O. *et al.* CD163-positive perivascular macrophages in the human CNS express molecules for antigen recognition and presentation. *Glia* **51**, 297–305 (2005).
14. Faraco, G. *et al.* Perivascular macrophages mediate the neurovascular and cognitive dysfunction associated with hypertension. *J. Clin. Invest.* **126**, 4674–4689 (2016).
15. Hawkes, C. A. & McLaurin, J. Selective targeting of perivascular macrophages for clearance of β-amyloid in cerebral amyloid angiopathy. *Proc. Natl. Acad. Sci.* **106**, 1261 LP – 1266 (2009).
16. Thanopoulou, K., Fragkouli, A., Stylianopoulou, F. & Georgopoulos, S. Scavenger receptor class B type I (SR-BI) regulates perivascular macrophages and modifies amyloid pathology in an Alzheimer mouse model. *Proc. Natl. Acad. Sci.* **107**, 20816 LP – 20821 (2010).
17. Polfliet, M. M. J. *et al.* The role of perivascular and meningeal macrophages in experimental allergic encephalomyelitis. *J. Neuroimmunol.* **122**, 1–8 (2002).
18. Zhang, Z. *et al.* Parenchymal accumulation of CD163+ macrophages/microglia in multiple sclerosis brains. *J. Neuroimmunol.* **237**, 73–79 (2011).
19. Chakarov, S. *et al.* Two distinct interstitial macrophage populations coexist across tissues in specific subtissular niches. *Science (80-.).* **363**, eaau0964 (2019).
20. Prinz, M. & Priller, J. Microglia and brain macrophages in the molecular age: from origin to neuropsychiatric disease. *Nat. Rev. Neurosci.* **15**, 300–312 (2014).
21. Utz, S. G. *et al.* Early Fate Defines Microglia and Non-parenchymal Brain Macrophage Development. *Cell* **181**, 557-573.e18 (2020).
22. Ydens, E. *et al.* Profiling peripheral nerve macrophages reveals two macrophage subsets with distinct localization, transcriptome and response to injury. *Nat. Neurosci.* **23**, 676–689 (2020).
23. Joseph, C. *et al.* Deciphering Hematopoietic Stem Cells in Their Niches: A Critical Appraisal of Genetic Models, Lineage Tracing, and Imaging Strategies. *Cell Stem Cell* **13**, 520–533 (2013).
24. Bazigou, E. *et al.* Genes regulating lymphangiogenesis control venous valve formation and maintenance in mice. *J. Clin. Invest.* **121**, 2984–92 (2011).
25. Brault, V. *et al.* Inactivation of the (β)-catenin gene by Wnt1-Cre-mediated deletion results in dramatic brain malformation and failure of craniofacial development. *Development* **128**, 1253 LP – 1264 (2001).
26. Jung, S. *et al.* Analysis of Fractalkine Receptor CX3CR1 Function by Targeted Deletion and Green Fluorescent Protein Reporter Gene Insertion. *Mol. Cell. Biol.* **20**, 4106–4114 (2000).

27. Back, J., Dierich, A., Bronn, C., Kastner, P. & Chan, S. PU.1 determines the self-renewal capacity of erythroid progenitor cells. *Blood* **103**, 3615–3623 (2004).
28. Li, J., Chen, K., Zhu, L. & Pollard, J. W. Conditional deletion of the colony stimulating factor-1 receptor (c-fms proto-oncogene) in mice. *genesis* **44**, 328–335 (2006).
29. Hägerling, R., Pollmann, C., Kremer, L., Andresen, V. & Kiefer, F. Intravital two-photon microscopy of lymphatic vessel development and function using a transgenic Prox1 promoter-directed mOrange2 reporter mouse. *Biochem. Soc. Trans.* **39**, 1674–81 (2011).
30. Madisen, L. *et al.* A robust and high-throughput Cre reporting and characterization system for the whole mouse brain. *Nat. Neurosci.* **13**, 133–140 (2010).
31. Renier, N. *et al.* iDISCO: A Simple, Rapid Method to Immunolabel Large Tissue Samples for Volume Imaging. *Cell* **159**, 896–910 (2014).
32. Engelhardt, B., Vajkoczy, P. & Weller, R. O. The movers and shapers in immune privilege of the CNS. *Nat. Immunol.* (2017). doi:10.1038/ni.3666
33. Ransohoff, R. M. & Engelhardt, B. The anatomical and cellular basis of immune surveillance in the central nervous system. *Nat. Rev. Immunol.* **12**, 623–635 (2012).
34. Hägerling, R. *et al.* A novel multistep mechanism for initial lymphangiogenesis in mouse embryos based on ultramicroscopy. *EMBO J.* **32**, 629–44 (2013).
35. Shibata-Germanos, S. *et al.* Structural and functional conservation of non-lumenized lymphatic endothelial cells in the mammalian leptomeninges. *Acta Neuropathol.* **139**, 383–401 (2019).
36. Bustelo, X. R., Suen, K. L., Leftheris, K., Meyers, C. A. & Barbacid, M. Vav cooperates with Ras to transform rodent fibroblasts but is not a Ras GDP/GTP exchange factor. *Oncogene* **9**, 2405–2413 (1994).
37. Lapenna, A., De Palma, M. & Lewis, C. E. Perivascular macrophages in health and disease. *Nat. Rev. Immunol.* (2018). doi:10.1038/s41577-018-0056-9
38. Koizumi, T., Kerkhofs, D., Mizuno, T., Steinbusch, H. W. M. & Foulquier, S. Vessel-Associated Immune Cells in Cerebrovascular Diseases: From Perivascular Macrophages to Vessel-Associated Microglia. *Front. Neurosci.* **13**, 1291 (2019).
39. Yang, T., Guo, R. & Zhang, F. Brain perivascular macrophages: Recent advances and implications in health and diseases. *CNS Neurosci. Ther.* **25**, 1318–1328 (2019).
40. Kösel, S. *et al.* Long-lasting perivascular accumulation of major histocompatibility complex class II-positive lipophages in the spinal cord of stroke patients: possible relevance for the immune privilege of the brain. *Acta Neuropathol.* **94**, 532–538 (1997).

41. Prinz, M. & Priller, J. The role of peripheral immune cells in the CNS in steady state and disease. *Nat Neurosci* **20**, 136–144 (2017).
42. Yona, S. *et al.* Fate Mapping Reveals Origins and Dynamics of Monocytes and Tissue Macrophages under Homeostasis. *Immunity* **38**, 79–91 (2013).
43. Lin, X. *et al.* An Ectoderm-Derived Myeloid-like Cell Population Functions as Antigen Transporters for Langerhans Cells in Zebrafish Epidermis. *Dev. Cell* **49**, 605-617.e5 (2019).

Competing Interests

The authors declare that the research was conducted in the absence of any commercial or financial relationships that could be construed as a potential conflict of interest.

Author Contributions

CS, ML, HWJ, MS, LF, AT, performed experiments. SAvdP conceived and supervised the study. CS, ML, HWJ, MS, and SAvdP analyzed data. CS, ML, HWJ, MS, AT, MF, SS, MHS, RS, RHA, SSM, FK and SAvdP contributed to discussion and wrote, illustrated, reviewed, and edited the manuscript. SAvdP acquired funding. All authors approved the submitted version of the manuscript.

Acknowledgments

The work was supported by the FRM Amorçage jeunes équipes (AJE20150633331), ANR ACHN (ANR-16-ACHN-0011), ANR PRCI (ANR-17-CE13-0029-01), A*midex Chaire d'excellence to SAvdP, DFG (FOR2325 to S.S.-M) and institutional grants to the CIML from INSERM, CNRS and Aix-Marseille University.

We acknowledge the PICSL imaging facility of the CIML (ImagImm), member of the national infrastructure France-BioImaging supported by the French National Research Agency (ANR-10-INBS-04), notably Mathieu Fallet and Sebastian Mailfert. Lionel Chasson of the histology platform for the relentless cutting. We thank the animal facility, notably Toufik Guelmami and Michel Pontier. The flow cytometry core facility, notably Marc Barad, Sylvain Bigot and Laurence Borge. We thank Hugues Lelouard and Marc Bajénoff for providing us with mouse models and Lydia Sorokin for the anti- Laminin γ1 antibody.

Data Availability Statement

All datasets generated for this study are included in the article/Supplementary Material. Single cell sequencing data is available under GSE133283.

FIGURE LEGENDS

Figure 1: Identification of a Lyve1^{+}CX3CR1^{-} population in the mouse brain. Confocal microscopy of brain sections stained with αLyve1 showing the different Lyve1^{+} cell morphologies in the superior cortex (17µm maximum intensity projection) **(A)**, in the inferior cortex (27µm maximum intensity projection) **(B)**, in the hippocampus (15µm maximum intensity projection) **(C)** and in the olfactory bulb (61µm maximum intensity projection) **(D)** of an adult mouse brain. **(E-I)** Immunofluorescence microscopy on sections of *Cx3cr1*^{GFP} and *Spi1*^{GFP} (encoding PU.1) in the superior cortex of the mouse brain. **(E)** Staining of *Cx3cr1*^{GFP} sections for Lyve1 (red) and F4/80 (50µm maximum intensity projection), **(F)** Iba1 (29µm maximum intensity projection), **(G)** CD45 (46µm maximum intensity projection, **(H)** Csf1R (34µm maximum intensity projection). (**I**) Staining of *Spi1*^{GFP} (PU.1 – green) sections for Lyve1 (red) and CD45 (37µm maximum intensity projection). White arrows point to conventional Lyve1^{+}CX3CR1^{+} pvM cells, which expressed F4/80^{+}, Iba1^{+}, CD45^{+} and Csf1R^{+}. The red arrows indicate Lyve1^{+}CX3CR1^{-} cells, which are F4/80^{+}, Iba1^{+}, CD45^{-} and Csf1R^{-} PU.1^{-}.

Figure 2: Perivascular Lyve1^{+} cell location. (A) Maximal projection (200µm maximum intensity projection) of a lightsheet microscope acquisition on a cleared mouse brain labeled for SMA (green), CD31 (red) and Lyve1 (blue). **(B)** Confocal microscopy of brain sections stained for Podoplanin (green), Lyve1 (red) and CD31 (blue), inserts **(C)** and **(D)** zoom in on Lyve1^{+} cells lining the blood vessels and placed outside of the « cul de sac of the pia mater » defined by the podoplanin labeling. **(E)** Confocal microscopy of a superior cortex section stained for CD31 (green), LaminininΫ1 (red) and Lyve1 (blue) with insert **(F)** showing a higher magnification showing the Lyve1^{+} cells in the perivascular space. **(G)** Lyve1^{+} cell characterization by immunofluorescence on adult brain sections for Lyve1 (green), VEGFR3 (red) and CD31 (blue) staining. The arrowhead points at a blood vessel and the white arrow shows a Lyve1^{+} cell negative for VEGFR3 and CD31. **(H)** high magnification of the Lyve1+ cell in **(G)**. **(I and J)** Lyve1^{+} cells (green) did not express Prox1 (red) in the superior cortex (39µm maximum intensity projection) nor in the inferior cortex (50µm maximum intensity projection) **(K and L)**.

Figure 3: Confirmation of the Lyve1^{+}CX3CR1^{-} population by flow cytometry. Flow cytometric analysis of *Cx3cr1*^{GFP} brain parenchyma, pre-gated on living, single and Lyve1^{+} cells. Microglia cells were excluded since these are Lyve1^{-}. Mouse brain were analyzed at **(A)** P2 (n= 4), **(B)** P7 (n=4), **(C)** P14 (n=4), **(D)** P21 (n=4), **(E)** Adult (8-12 weeks after birth, n= 4) and **(F)** 1-year old brains (n=3)

showing subsequent CX3CR1, F4/80 expression for the cells of the $CD45^{Int}$ and $CD45^{-}$ gates. **(G)** Total number of $Lyve1^{+}CD45^{-}CX3CR1^{-}F4/80^{+}$ cells at the different stages.

Figure 4: Transcriptional profiling of the pvM subsets. A) Quantification by RT-QPCR of the relative expression of *Ptprc* (encoding CD45) within the CD45 cell subpopulations ($CD45^{-}$ for CD45 negative, CD45 I for intermediate and CD45 H for high expressing CD45) isolated from C57BL/6J brain parenchyma (3 sorts with n=5 mice per sort), **(B)** Single cell RNA sequencing of non-neuronal population, focused on the macrophage subset, revealed two main populations. **(D)** A segregation occurred between a $Lyve1^{+}$ vs. MHCII (e.g. *H2-Aa*) macrophage subsets, visualized in the individual gene expressions plotted within the tSNE plots. *Ptprc* and *Cx3cr1* transcripts were present in few cells while *Spi1* (encoding PU.1) transcripts were present in more Lyve1 and MHCII cells.

Figure 5: Origin of $Lyve1^{+}$ cells. (A) Immunofluorescence on sections of the head of a E18.5 $Spi1^{GFP/+}$ embryo, labeled for Lyve1 (red) and CD45 (60µm maximum intensity projection) shows the presence of the conventional (white arrows) and the non-conventional pvM population (red arrows) at this stage. **(B)** No GFP nor Lyve1 fluorescence was observed in the $Spi1^{GFP/GFP}$ E18.5 superior cortex (33µm maximum intensity projection). **(C)** Confocal analysis of Vav^{tdT} (26µm maximum intensity projection) brain sections stained for Lyve1 (green) and CD45 (white). White arrows indicate the conventional pvM population, which is tdT positive (red) and the red arrows the $CD45^{-}CX3CR1^{-}$ population which is tdT negative.

Figure 6: pvM2 share phagocytic functioning with conventional pvM. (A-C) $Cx3cr1^{GFP}$ mouse brains were injected intra-ventricular with Dextran-Alexa647 (37µm maximum intensity projection) and **(D-F)** Acetylated-LDL-Alexa594 (42µm maximum intensity projection). Ten minutes after injection, mice were sacrificed and brains dissected. Confocal analysis on brain sections shows Lyve1 (white), Dyes (red) and CX3CR1 (green). The pvMs phagocytosed the dyes (red arrows), as well as did conventional pvM (white arrows) **(B, C, E and F)**. **(G)** Tiled confocal acquisition of a $Prox1^{mOrange2}$ brain section. $Lyve1^{+}$ cells in green lined blood vessels stained for CD31 in blue. $Lyve1^{+}$ cells in green penetrated the brain to the hippocampal fissure (hif) and all the way towards the third ventricle (3V).

Figure 7: pvM2 increase in numbers after induced ischemic stroke. (A) Maximal intensity projections (2660µm) of lightsheet acquisitions on cleared brains, stained for Lyve1 (red) and CD45 (white), control and after stroke (P14=14 days after induction of ischemic stroke). **(B)** Quantification

of Lyve1 in the area containing the whole stroke lesion within the superior cortex situated just above the hippocampus, imaged by lightsheet microscopy. **(C)** Representative flow cytometry plots from *Cx3cr1*^{GFP} brain parenchyma 14 days after induced stroke (P14), pre-gated on living, single and Lyve1^{+} cells. Microglia cells were excluded since they are Lyve1^{-}. CX3CR1 vs F/80 expression is shown for the CD45^{-} population. Average percentages for the different subpopulations are shown in the plots (n=4). **(D)** Graph representing the total Lyve1^{+} cell number showing an increase of this population at P14 after stroke by flow cytometry. **(E)** Total pvM2 (Lyve1^{+}CD45^{-}CX3CR1^{-}F4/80^{+}) numbers in the control vs. PT brains at P14.

SUPPLEMENTARY MATERIALS

Table 1: Ab Resources Table for Imaging (confocal and lightsheet microscopy)

Table 2: pvM vs pvM2 markers

Supplementary Figure 1: pvM2 characterization. (A) Lightsheet imaging of a cleared adult C57BL/6J mouse brain immunolabeled with αLyve1 using iDisco+ protocol (5550µm maximum intensity projection), related to video 1. **(B-C)** Immunofluorescence microscopy on brain parenchyma sections of **(B)** *Spi1*^{GFP} and **(C)** *Cx3cr1*^{GFP} in the superior cortex, using an anti-GFP to enhance the GFP signal (green) with Lyve1 staining labeled in red. **(D-G)** Brain sections are labeled for Lyve1 (green) and for **(D)** CD163 (16µm maximum intensity projection), **(E)** CD206 (48µm maximum intensity projection), **(F)** MHCII (35µm maximum intensity projection), **(G)** CD11b (85µm maximum intensity projection) (red). White arrows show the conventional pvM population and red arrows show the non-conventional pvM population.

Supplementary Figure 2: Lyve1$^+$ cells are neither lymphatic endothelial cells (LEC), nor astrocytes, nor fibroblasts. (**A)** 1080µm maximum intensity projection of lightsheet microscope acquisition of the superior cortex illustrating the « cul de sac of the pia mater » defined by the podoplanin labeling, structure emanating from the pia mater (CD31 in green, Lyve1 in red and Podoplanin in blue). **(C)** Confocal analysis of *Prox-CreERT2*$^{+/-}$; *Rosa*^{tdTomato} brain sections stained for Lyve1 (green) confirmed that Lyve1$^+$ cells do not express tdTomato (red) (white arrows) (88µm maximum intensity projection). (**D)** LEC identification (Lyve1$^+$ Prox1$^+$) in the pia mater in the superior cortex by Prox1 antibody staining (red) on C57BL/6J mouse brain in combination with Lyve1 (green). Prox1$^+$ neuron cellular bodies are observed in the parenchyma (13µm maximum intensity projection). **(E)** Astrocyte identity was excluded by AQP4 and GFAP (red) staining (24µm maximum intensity projection for the superior cortex and 17µm maximum intensity projection for the inferior cortex), **(F)** fibroblast identity was excluded by ER-TR7 staining (50µm maximum intensity projection for the superior cortex and 8µm maximum intensity projection for the inferior cortex) and **(G)** PDGFRβ (red) staining. **(H)** Confocal analysis of *Wnt-Cre; Rosa26*^{tdTomato} (37µm maximum intensity projection) brain sections stained for Lyve1 (green), containing tdTomato (red). White arrows indicate the Tomato negative CD45$^-$CX3CR1$^-$ perivascular cells.

Supplementary Figure 3: Confirmation of the Lyve1^{+}CX3CR1^{-} population by flow cytometry **(A)** Flow cytometry gating strategy. **(B)** CD45^{High} cells from *Cx3cr1^{GFP}* brain parenchyma, pre-gated on living, single and Lyve1^{+} cells. Microglia cells were excluded as Lyve1^{-}. Mouse brain analysis at different ages P2 (n= 4), P7 (n=4), P14 (n=4), P21 (n=4), Adult (8-12 weeks) (n=4), and 1 year old, (n=3) showing subsequent CX3CR1, F4/80 expression for the cells of the CD45^{High} gates. Gating of pvM identified as Lyve1^{+}CD45^{High} isolated from *Cx3cr1^{GFP}* brain parenchyma. (C) Flow cytometry analysis of CD45 cell subpopulations isolated from *Spi1^{GFP}* adult brain parenchyma (8-12 weeks after birth, n= 4) , pre-gated on living, single and Lyve1^{+} cells. Microglia cells were excluded as Lyve1^{-}. Plots show subsequent PU.1, F4/80 expression for the CD45^{Int}, CD45^{Neg} and CD45^{High} gates.

Supplementary Figure 4: Gene expression profiling (A) Sort gating strategy for the isolation of the different Lyve1^{+}CD45 populations **(B)**. Single RNA sequencing analysis showing different macrophage associated genes within the tSNE plots.

Supplementary Figure 5: Immunofluorescence of the section of a E18.5 head from a *Spi1$^{GFP/+}$* embryo (PU.1-GFP in green), labeled for Lyve1 (red) and CD45 (white). No GFP or Lyve1 fluorescence was observed in the *Spi1$^{GFP/GFP}$* E18.5 superior cortex (33µm maximum intensity projection) but we observed Lyve1^{+} cells, possibly lymphatic vessels, in the skull.

Supplementary Figure 7: Lightsheet data quantification method using Imaris software. (A) To quantify the Lyve1 staining in cleared brains imaged by lightsheet microscopy, Imaris software was used. Using the "Surface tool" of Imaris, a 3D Rendering function, a first volume was created, named « Surface1 » at different locations (Superior cortex and hippocampus) where we wanted to quantify the staining. Based on Lyve1 labelling, a new channel was created. This new channel was used to create a new volume called « Surface 2 » representing the Lyve1 staining. Imaris calculated the different volumes in µm^3. The ratio « Surface2 » / « Surface1 » allows us to normalize the Lyve1 quantification. **(B)** Gating of conventional pvM identified as Lyve1^{+}CD45^{int} and as Lyve1^{+}CD45^{High} isolated from *Cx3cr1^{GFP}* brain parenchyma at P14 after stroke.

Supplementary Video 1: 3D reconstruction of Lyve1 cells within the mouse brain. A cleared sagittal half of an adult C57BL/6J mouse brain immunolabeled for Lyve1 (red) was acquired on the lightsheet microscope and a 3D reconstruction was made using Imaris. The video zooms in on the inferior cortex and subsequently on the hippocampus to indicate the differences in pvM morphology

within these regions.

Supplementary Video 2: Z-stack acquisition by confocal microscopy and 3D reconstruction of the pvM morphology adjacent to a blood vessel within the brain parenchyma. A 100µm brain section was stained with αLyve1 (red) and αCD31 (green). 3D reconstruction was done using the Imaris surface tool and the video was created using the animation function of Imaris.

Figure 1

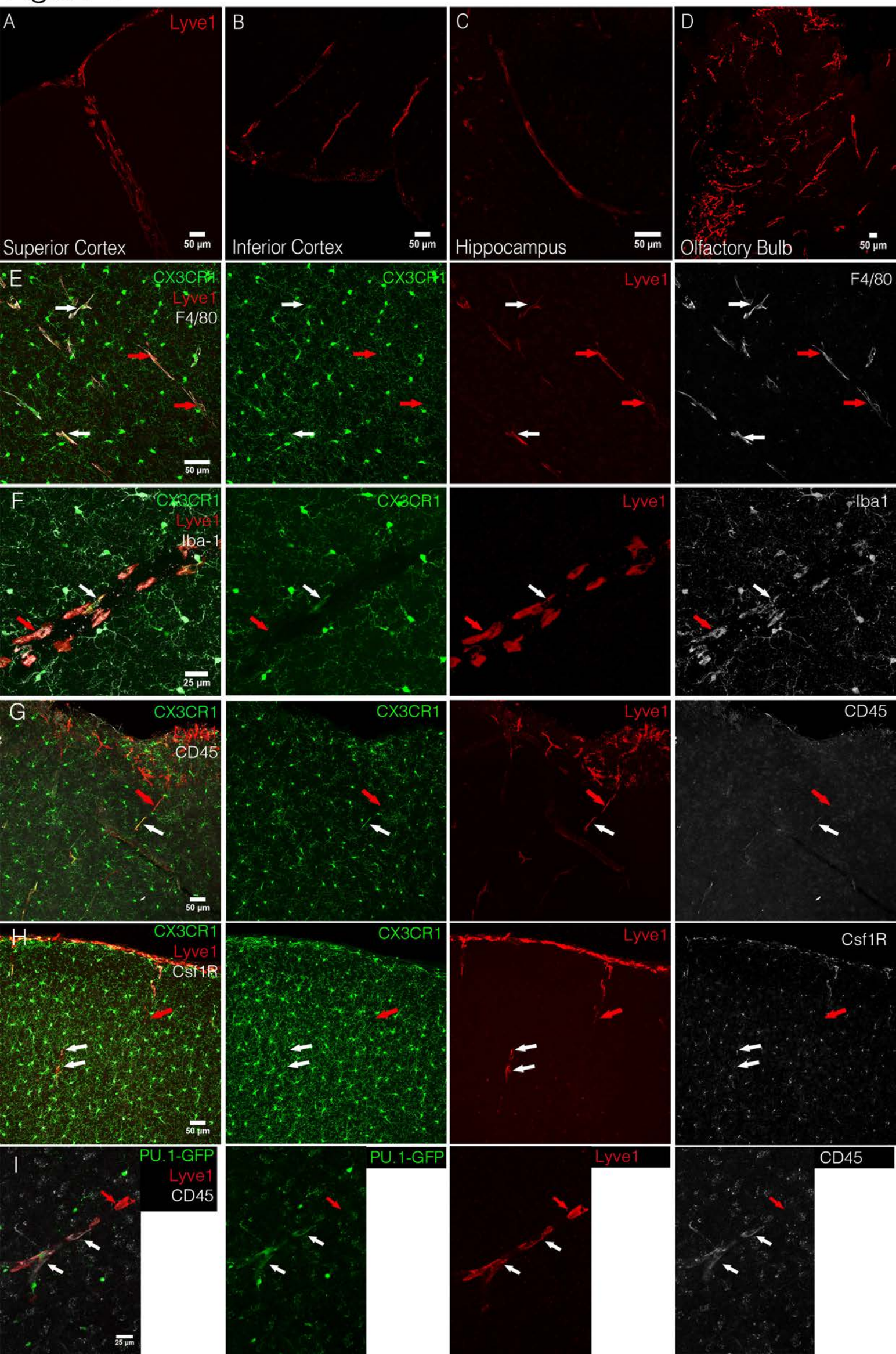
A
Lyve1
Superior Cortex
50 µm
B
Inferior Cortex
50 µm
C
Hippocampus
50 µm
D
Olfactory Bulb
50 µm
E
CX3CR1
Lyve1
F4/80
50 µm
CX3CR1
Lyve1
F4/80
F
CX3CR1
Lyve1
Iba-1
25 µm
CX3CR1
Lyve1
Iba1
G
CX3CR1
Lyve1
CD45
50 µm
CX3CR1
Lyve1
CD45
H
CX3CR1
Lyve1
Csf1R
50 µm
CX3CR1
Lyve1
Csf1R
I
PU.1-GFP
Lyve1
CD45
25 µm
PU.1-GFP
Lyve1
CD45

Figure 2

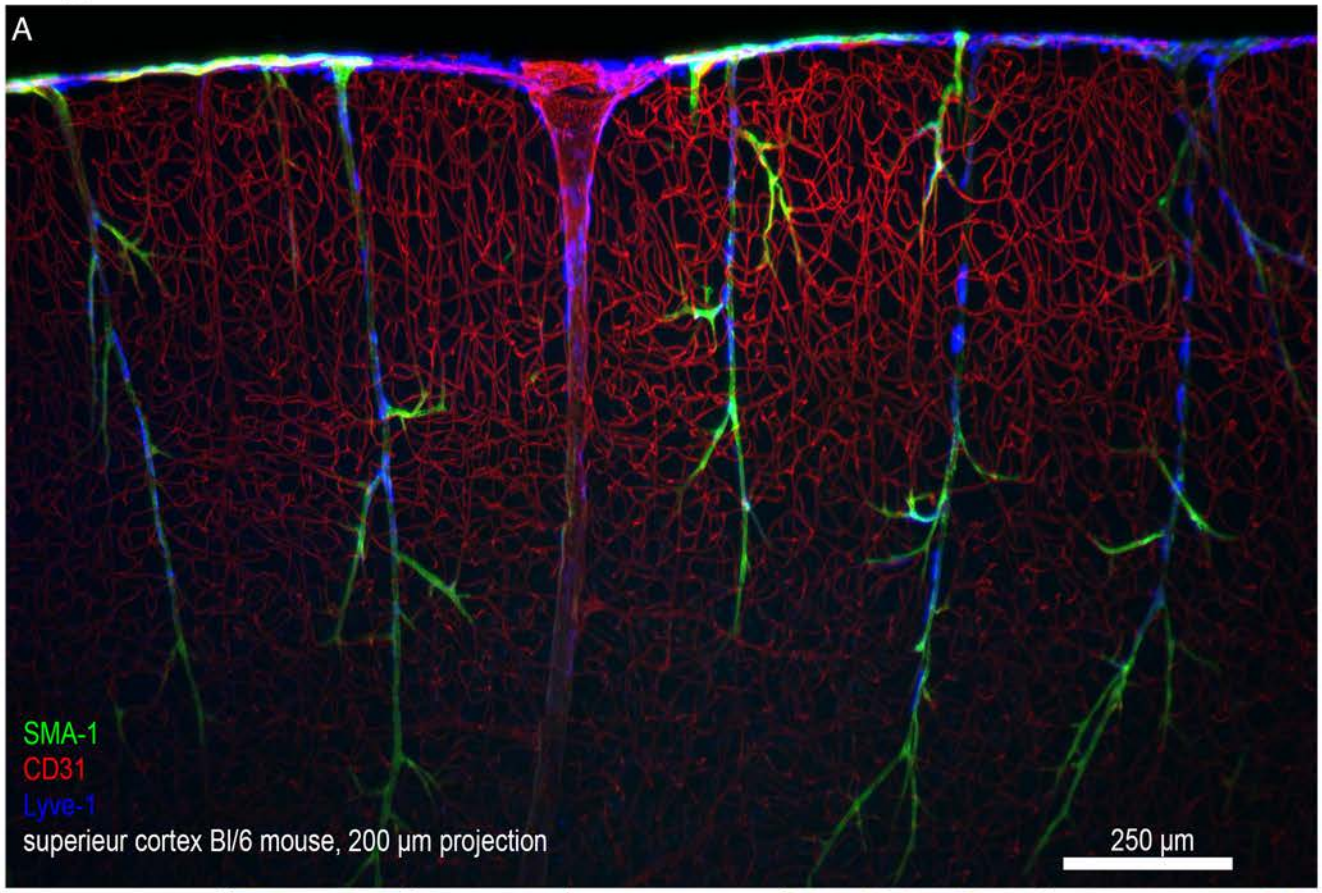
A
SMA-1
CD31
Lyve-1
superieur cortex Bl/6 mouse, 200 µm projection
250 µm

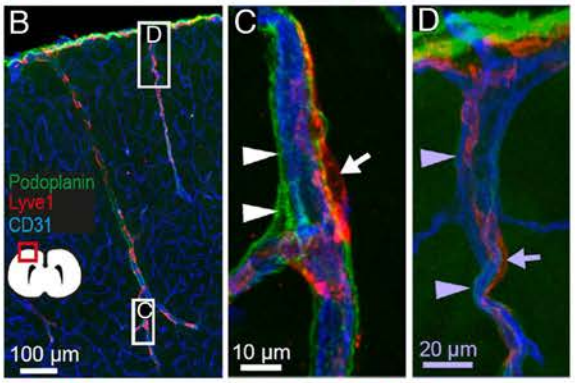
B
D
Podoplanin
Lyve1
CD31
C
100 µm
C
10 µm
D
20 µm

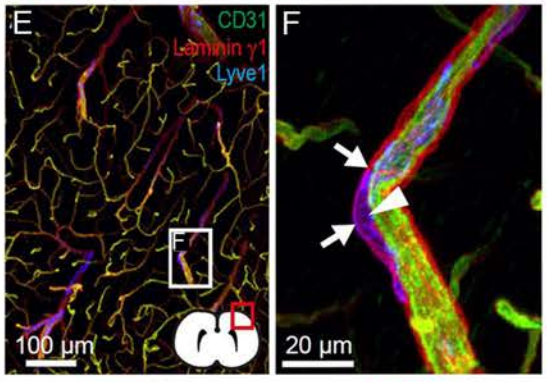
E
CD31
Laminin γ1
Lyve1
F
100 µm
F
20 µm

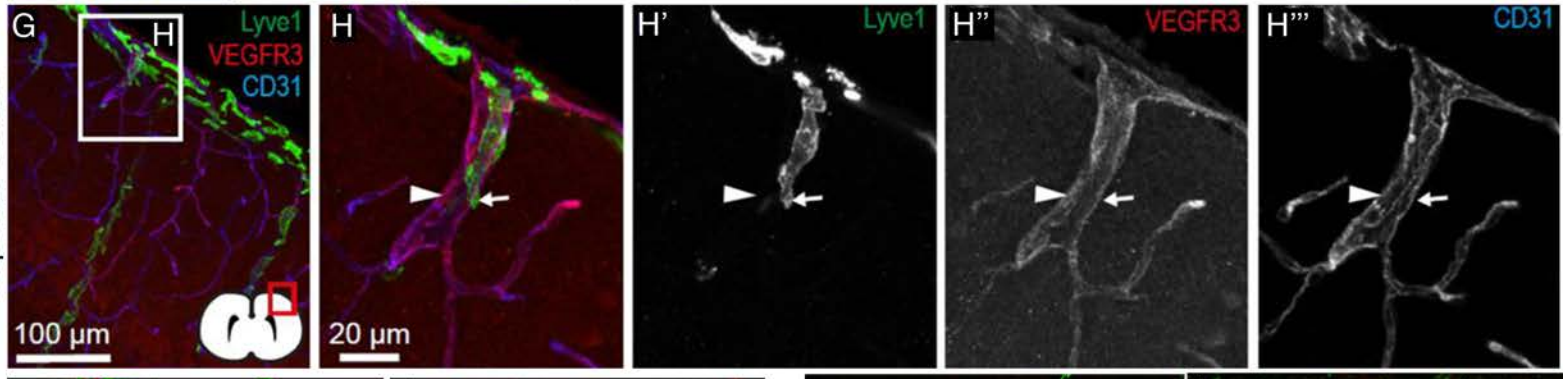
Superior Cortex
G
H
Lyve1
VEGFR3
CD31
100 µm
H
20 µm
H'
Lyve1
H''
VEGFR3
H'''
CD31

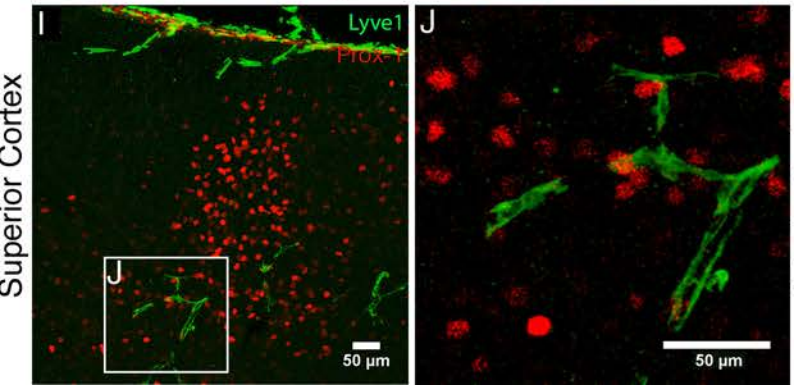
Superior Cortex
I
Lyve1
Prox-1
J
50 µm
J
50 µm

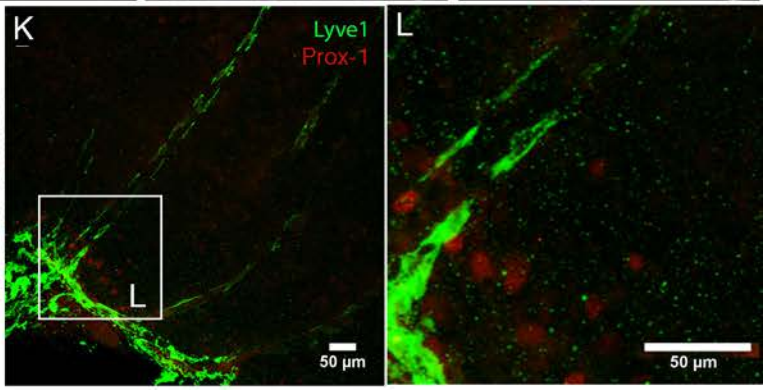
Inferior Cortex
K
Lyve1
Prox-1
L
50 µm
L
50 µm

Figure 3

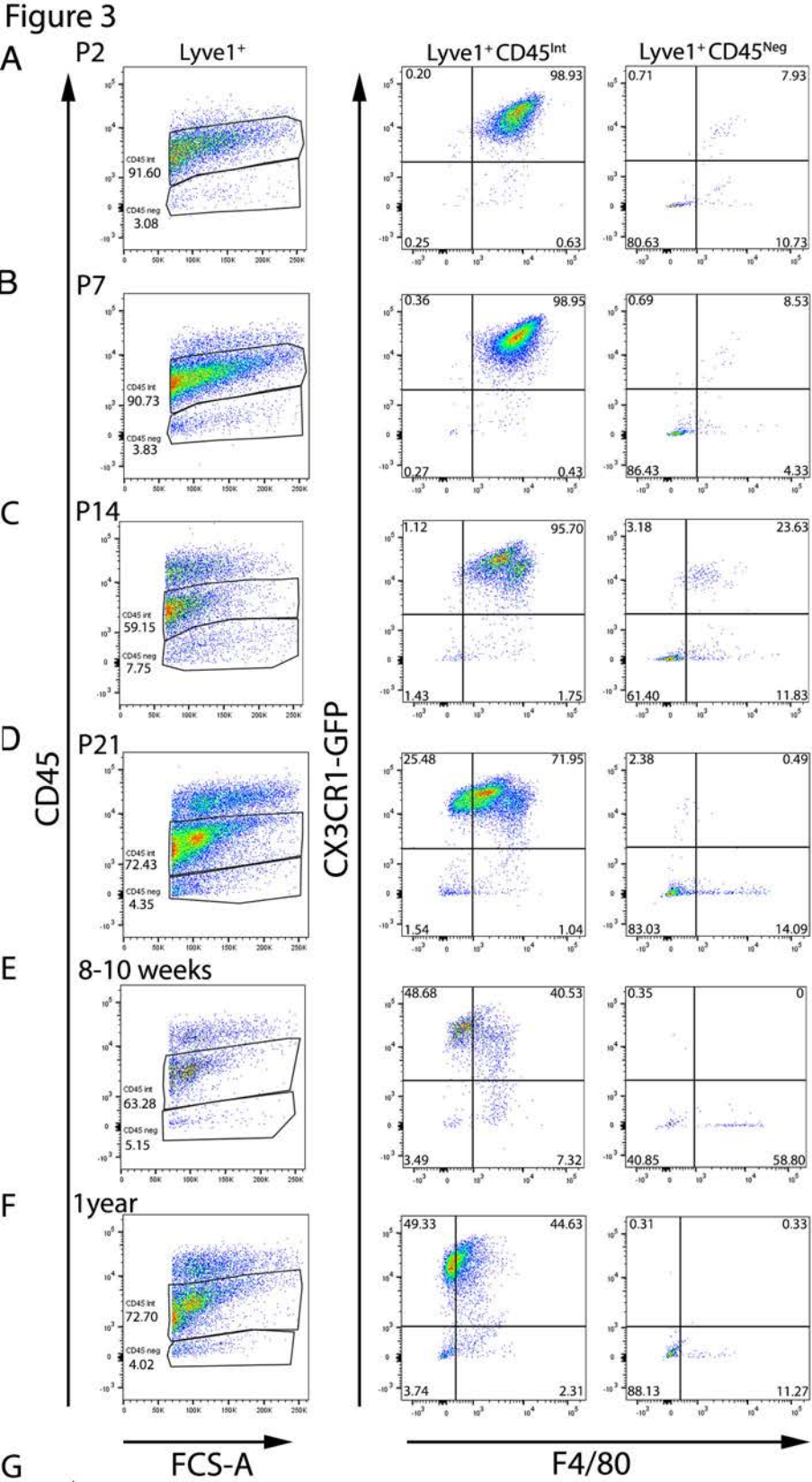
A
P2
Lyve1+
Lyve1+CD45Int
Lyve1+CD45Neg
CD45 int
91.60
CD45 neg
3.08
0.20
98.93
0.25
0.63
0.71
7.93
80.63
10.73
B
P7
CD45 int
90.73
CD45 neg
3.83
0.36
98.95
0.27
0.43
0.69
8.53
86.43
4.33
C
P14
CD45 int
59.15
CD45 neg
7.75
1.12
95.70
1.43
1.75
3.18
23.63
61.40
11.83
D
P21
CD45 int
72.43
CD45 neg
4.35
25.48
71.95
1.54
1.04
2.38
0.49
83.03
14.09
CD45
CX3CR1-GFP
E
8-10 weeks
CD45 int
63.28
CD45 neg
5.15
48.68
40.53
3.49
7.32
0.35
0
40.85
58.80
F
1year
CD45 int
72.70
CD45 neg
4.02
49.33
44.63
3.74
2.31
0.31
0.33
88.13
11.27
FCS-A
F4/80
G
Lyve1+CD45-CX3CR1+F4/80+ cell number
200
150
100
50
0
p=0,0005
p=0,04
P2
P7
P14
P21
8-10 weeks
1 year

Figure 4

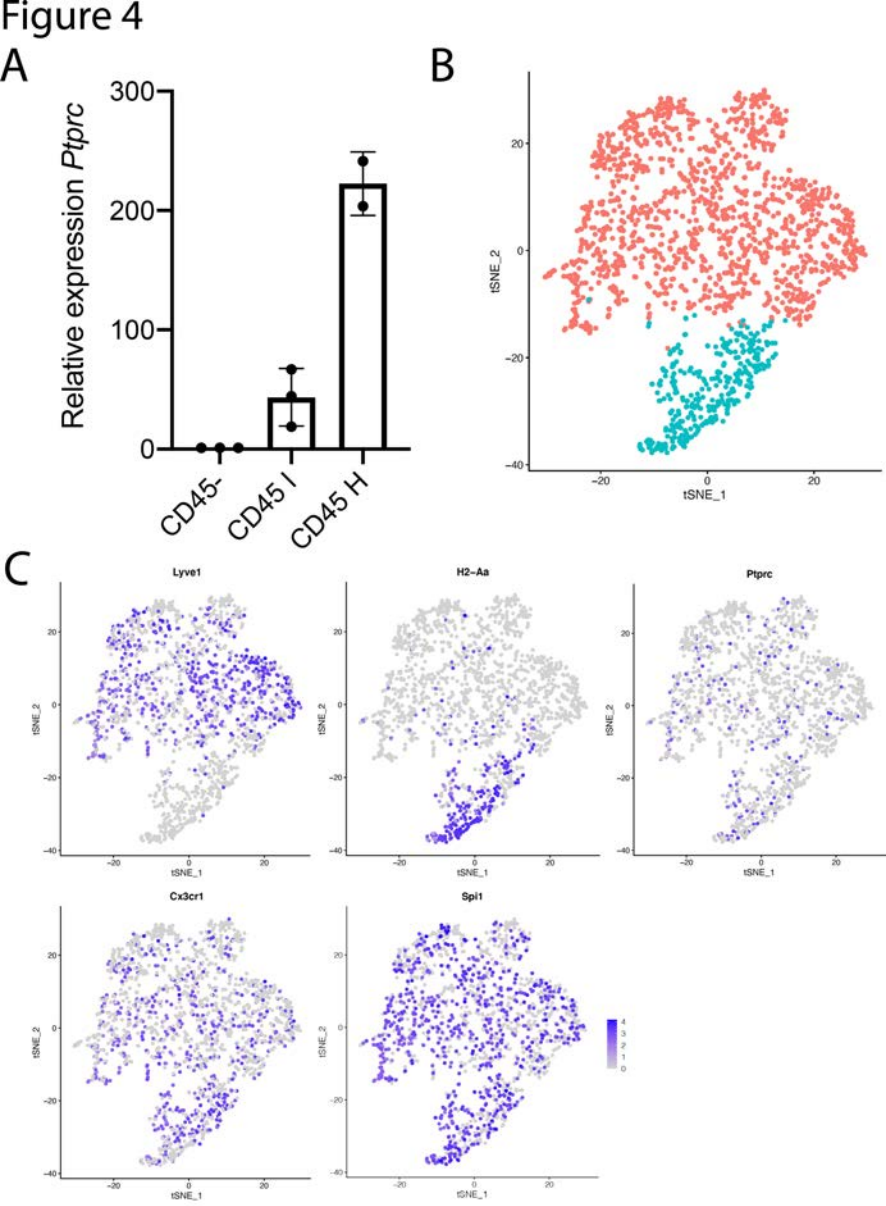
A
Relative expression Ptprc
300
200
100
0
CD45-
CD45 l
CD45 H
B
tSNE_2
tSNE_1
C
Lyve1
H2-Aa
Ptprc
Cx3cr1
Spi1
tSNE_2
tSNE_1

Figure 5

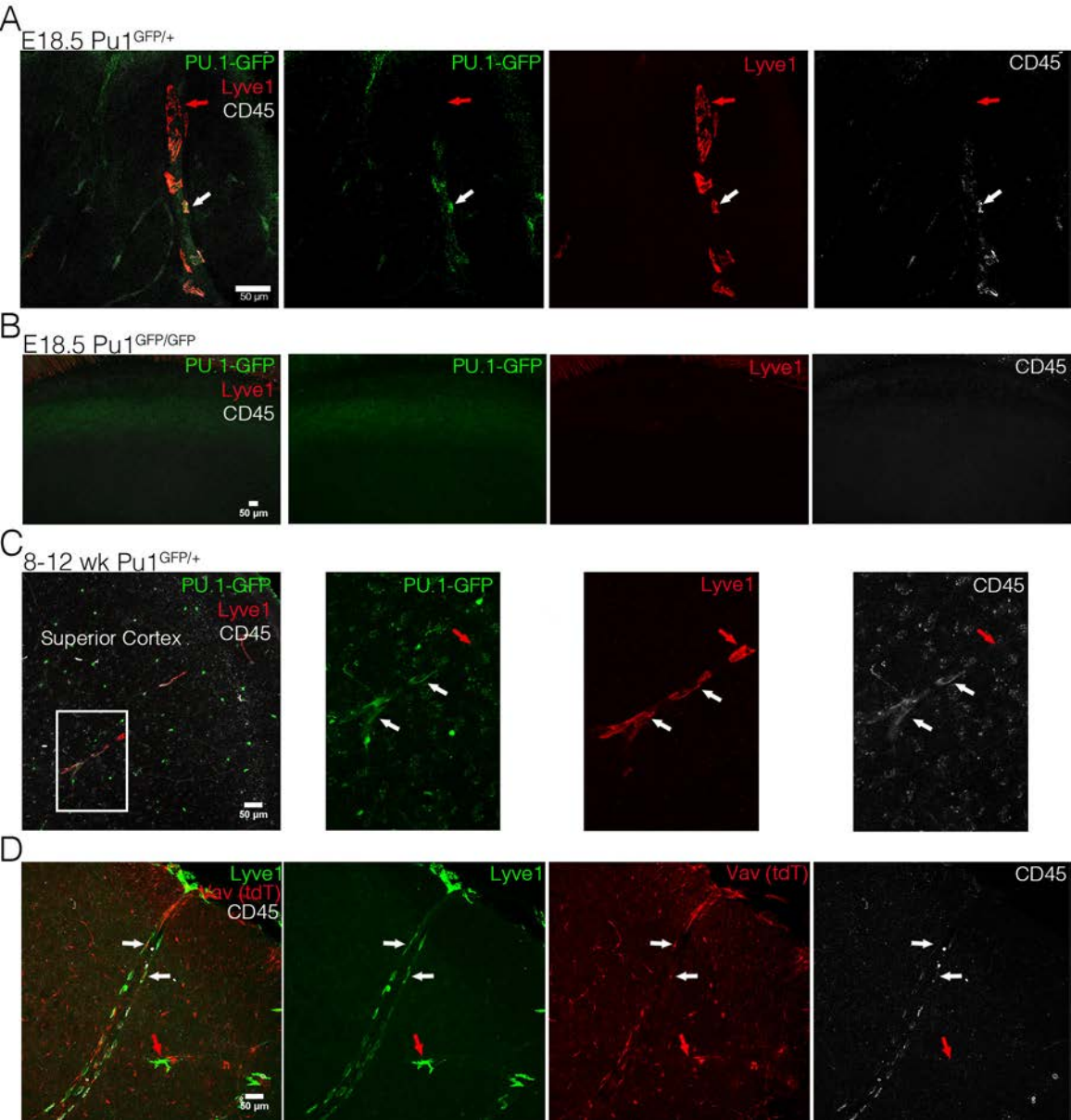
A
E18.5 Pu1GFP/+
PU.1-GFP
Lyve1
CD45
50 µm
B
E18.5 Pu1GFP/GFP
C
8-12 wk Pu1GFP/+
Superior Cortex
D
Vav (tdT)

Figure 6

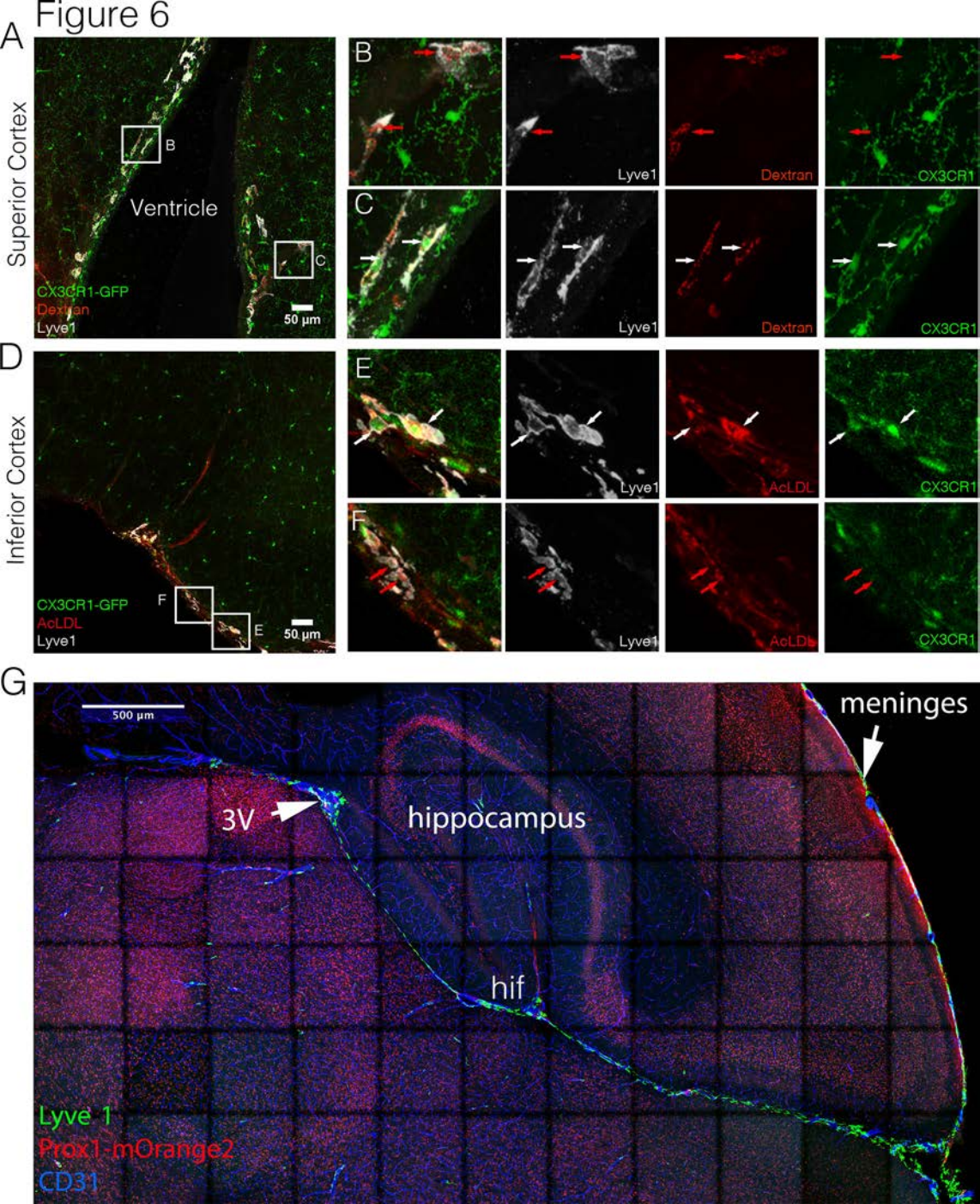
A
Superior Cortex
B
Ventricle
C
CX3CR1-GFP
Dextran
Lyve1
50 µm
B
Lyve1
Dextran
CX3CR1
C
Lyve1
Dextran
CX3CR1
D
Inferior Cortex
CX3CR1-GFP
AcLDL
Lyve1
F
E
50 µm
E
Lyve1
AcLDL
CX3CR1
F
Lyve1
AcLDL
CX3CR1
G
500 µm
meninges
3V
hippocampus
hif
Lyve 1
Prox1-mOrange2
CD31

Figure 7

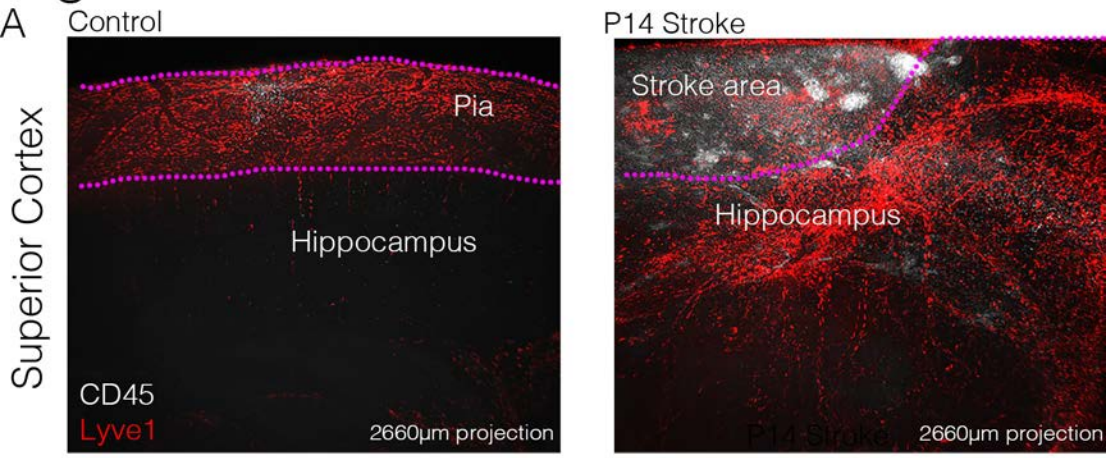
A
Control
Superior Cortex
Pia
Hippocampus
CD45
Lyve1
2660µm projection
P14 Stroke
Stroke area
Hippocampus
P14 Stroke
2660µm projection

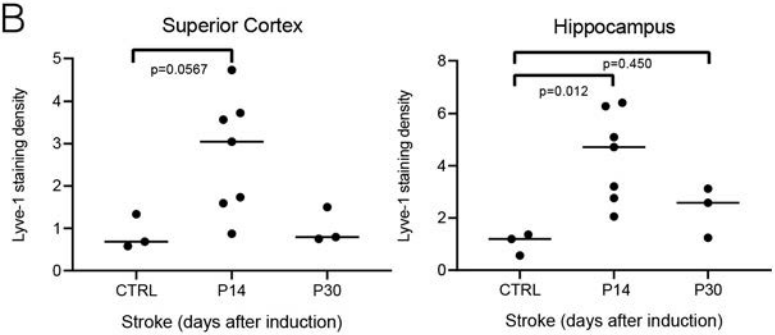
B
Superior Cortex
p=0.0567
Lyve-1 staining density
CTRL
P14
P30
Stroke (days after induction)
Hippocampus
p=0.450
p=0.012
Lyve-1 staining density
CTRL
P14
P30
Stroke (days after induction)

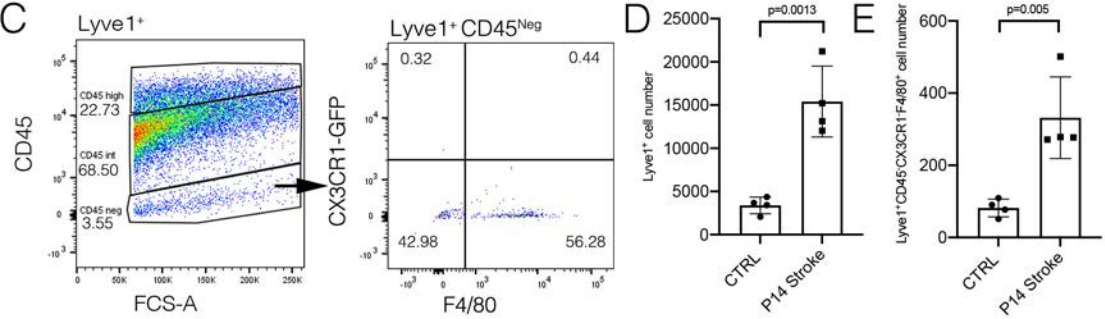
C
Lyve1+
CD45
CD45 high
22.73
CD45 int
68.50
CD45 neg
3.55
FCS-A
Lyve1+ CD45Neg
CX3CR1-GFP
0.32
0.44
42.98
56.28
F4/80
D
p=0.0013
Lyve1+ cell number
CTRL
P14 Stroke
E
p=0.005
Lyve1+CD45-CX3CR1-F4/80+ cell number
CTRL
P14 Stroke

Table 1
Ab Ressources Table for Imaging
(confocal and Lightsheet)

Primary Antibodies	Source	Identifier
Lyve-1	R&D systems	AF2125
AQP4	R&D systems	AB3594
GFAP	Biolegend	644706
CD45	eBioscience	14-0451-85
MHCII	BD Pharmingen	562352
F4/80	Biolegend	123122
Iba1	Abcam	ab107159
CD163	Anders	homemade
CD11b	eBioscience	16-0112-82
CD206	Thermofisher	48-2061-82
CD31	Thermo	MA1-40074
Prox-1	Reliatech	102-PA32
VEGFR3	R&D systems	AF743
α-SMA	Thermofisher	53-9760-82
PDGFRβ	Cell Signaling	3169S
ER-T7R	Thermofisher	MA1-40076
Csf-1R	Santa Cruz	sc-692
GFP	AVES	GFP-1020
Laminin γ1	Sorokin L (University of Muenster)	

Secondary Antibodies	Source	Identifier
DaChCy3	Jackson ImmunoResearch	703-166-155
DaG 488	Thermofisher	A-11055
DaG 555	Thermofisher	A-21432
DaG 647	Thermofisher	A-21447
DaG 790	Jackson ImmunoResearch	712-655-153
DaR 488	Thermofisher	A-21208
DaR 594	Thermofisher	SA5-10028
DaR 647	Jackson ImmunoResearch	712-605-153
DaRb 488	Thermofisher	A-21206
DaRb 555	Thermofisher	A-31572
DaRb 647	Jackson ImmunoResearch	711-605-152

Table 2

Conventional pvM	pvM2
Lyve1^{+}	Lyve1^{+}
CD45^{+}	CD45^{-}
CX3CR1^{+}	CX3CR1^{-}
PU1^{+}	PU1^{-}
Csf1R^{+}	Csf1R^{-}
F4/80^{+}	F4/80^{+}
Iba1^{+}	Iba1^{+}
CD163^{+}	CD163^{-}
CD11b^{+}	CD11b^{-}
CD206^{+}	CD206^{-}
MHCII^{+}	MHCII^{-}

Supplementary Files

This is a list of supplementary files associated with this preprint. Click to download.

- pvM2SiretetalSupplFig.pdf
- Video1Lyveinbrainzoominfcortexandhc720.mov
- Video2cd31lyve13dvessel720.mov